PNAS RESEARCH ARTICLE | ENGINEERING

Wireless arm-worn bioimpedance sensor for continuous assessment of whole-body hydration

Matija Jankovic[a], Seungmin Kang[b], Sarnab Bhattacharya[a], Jordon Kashanchi[a], Jieting Wang[c], Kanika Deoli[a], Tianda Huang[a], Alex Johnson[a], Karina Ambani[b], Sangjun Kim[d], Pulin Wang[e], Edward Coyle[c], and Nanshu Lu[a,b,f,g,1]

Affiliations are included on p. 11.

Edited by Yonggang Huang, Northwestern University-Evanston, Glencoe, IL; received February 24, 2025; accepted June 10, 2025

Assessment of whole-body hydration (WBH) is crucial for health management and disease diagnosis. Traditional methods are invasive or require bulky equipment, making them impractical for mobile, continuous sensing. We present a wearable bioimpedance sensor with strategic electrode placement across the arm for noninvasive, continuous, and mobile WBH monitoring. Although whole-body bioimpedance is a proven method for indicating WBH, the effectiveness of local bioimpedance measurement has been unclear. Our finite element analysis demonstrated that with an optimized cross-arm sensing configuration, a strong linear relationship exists between arm bioimpedance and muscle electrical resistivity, confirming the utility of arm bioimpedance for assessing WBH given the well-established relationship between muscle electrical resistivity and body water. Our IRB-approved diuretic-induced dehydration study demonstrated a strong linear correlation between the increase of arm bioimpedance and the decrease in body weight due to water loss, with a Pearson correlation coefficient of 0.956 ± 0.033 among eight participants. Arm and whole-body demonstrated strong alignment, suggesting that arm bioimpedance measurements can reflect not only changes in WBH but also potentially absolute WBH status when compared against established population reference data. In a 24-h free-living experiment, the wireless, dry electrode-based, arm-conformable bioimpedance sensor continuously tracked dehydration and rehydration despite motions associated with daily activities. These results suggest that properly measured arm bioimpedance can serve as a surrogate for WBH, offering a reliable and accessible solution. The potential uses of this wearable technology range from improving personal wellness to enhancing professional sports and occupational safety.

dehydration | bioimpedance | wearable electronics | flexible electronics | bioelectrical impedance vector analysis

Significance

Hydration is essential for human health and bodily function. Dehydration impairs cognition and physical performance and can lead to serious conditions such as kidney stones and chronic disease. State-of-the-art methods offer only momentary snapshots of whole-body hydration (WBH), lacking the ability to inform prompt rehydration or other necessary interventions. To address this unmet need, we created a wireless cross-arm bioimpedance sensor capable of continuous and ambulatory monitoring of WBH in everyday life. IRB-approved dehydration tests revealed strong correlations between the change in arm bioimpedance and body water loss. The bioelectrical impedance vector analyses (BIVA) of the arm and entire body also showed high consistency. This wearable technology is significant in raising awareness of dehydration and enabling proactive health management.

Water is vital for the human body: it constitutes 45 to 70% of human body mass, facilitates oxygen and nutrient transport, maintains proper organ function, regulates body temperature, eliminates waste, and supports virtually all other vital physiological processes (1, 2). Dehydration, defined as a deficit in total body water (TBW), is a common but often overlooked condition. It can arise from inadequate fluid intake, excessive sweating, vomiting, and/or diarrhea (3). Initial symptoms, such as headache and dry mouth, can escalate to more serious conditions if left untreated. The severity of dehydration can be quantified by the percentage change in total body weight caused by water loss. For example, life-threatening symptoms, such as altered respiratory activity or various cardiovascular conditions (e.g., low blood pressure, elevated heart rate), can arise with a 1 to 2% body weight loss and become pronounced with a 3 to 5% loss (4). Considerable cognitive impairment has been observed to begin with a 2% reduction in body weight due to water loss (5, 6). Dehydration also affects the thermoregulatory capacity of the body by decreasing sweating and cutaneous blood flow. For instance, core body temperature increases by 0.15 to 0.20 °C for every 1% decrease in body weight due to fluid loss (7). Reduced thermoregulation increases the risk of developing heat-related injuries, such as muscle cramps, fatigue, or heatstroke (8). Chronic mild dehydration is associated with an increased risk of kidney stone formation (9, 10).

Unfortunately, while the negative effects of dehydration and the importance of rehydration are well known, a significant portion of the population is still at risk. For example, persons working in extreme temperature environments (e.g., firefighters, armed forces personnel) are more likely to experience dehydration. The estimated fluid loss for these individuals may exceed 1 L/h solely by perspiration (11). Athletes are also susceptible

The authors declare no competing interest.

This article is a PNAS Direct Submission.

[1]To whom correspondence may be addressed. Email: nanshulu@utexas.edu.

This article contains supporting information online at https://www.pnas.org/lookup/suppl/doi:10.1073/pnas.2504278122/-/DCSupplemental.

Published July 14, 2025.

to dehydration due to increased sweat production, which can exceed 1 L/h (3). When combined with heat stress, dehydration significantly impairs cognitive functions, athletic performance, and technical skills related to sports (12). Even minor levels of dehydration can be critical, particularly at the elite level. Consequently, athletes, firefighters, and armed forces personnel would greatly benefit from continuous hydration assessment as a means of optimizing performance, preventing injury, and aiding recovery.

Common practices for assessing dehydration typically involve qualitative methods, such as comparing the physical appearance of urine with a color chart (Fig. 1 *A*, *i*) (2). However, these methods are susceptible to human errors and contamination (e.g., food, medicines) and are unsuitable for monitoring rapid changes in hydration status. Quantitative assessment of a person's WBH level is usually based on blood or urine tests, such as blood, serum, plasma, or urine osmolality tests in laboratories (13) (Fig. 1 *A*, *ii*). Although these results are accurate, they are time-consuming and costly and only offer intermittent data points. The lack of a mobile, real-time WBH assessment approach hinders timely decision making and the initiation of necessary rehydration measures.

Bioelectrical impedance (bioimpedance or Bio-Z) provides a noninvasive and quantitative approach to evaluate WBH (2, 14, 15). Bioimpedance analysis (BIA) capitalizes on the deep tissue penetration capability of alternating current (AC) to extract valuable physiological information (16–19). At low frequencies, AC predominantly traverses the ECF due to the capacitive properties of cell membranes, whereas at higher frequencies, the reduced capacitive reactance allows current to penetrate cell membranes, enabling it to flow through both ECF and ICF (Fig. 1*B*) (16). Therefore, when Bio-Z is measured across a multitude of frequencies, known as bioimpedance spectroscopy (BIS), it can distinguish between ECF and ICF (14). Commercial equipment for WBH assessment typically requires placing electrodes on the hands and feet to measure whole-body Bio-Z (Fig. 1 *A*, *iii*), but such equipment is stationary, expensive, and impractical for daily use. Wearable BIS sensors for WBH assessment are emerging (20), but they continue to use gel-based electrodes that are widely known to dehydrate and degrade signal quality over time (21). Furthermore, BIA and BIS estimate fluid volumes, such as ECF and TBW, using regression equations that incorporate parameters like gender, age, and weight which can induce significant errors (22). An improved approach, named BIVA, separates the resistance (R) and reactance (X_c) components of Bio-Z (23) and uses the vectorial changes in the plot $R - X_c$ to chart changes in hydration and body composition (Fig. 1*C*) (24–30). The National Health and Nutrition Examination Survey III (NHANES III) recorded the whole-body electrical resistance and reactance of a healthy reference population of 7,722 men and 8,181 women to provide a qualitative indication of hydration, without making assumptions about body components or prediction models (24, 25). The confidence ellipses in a BIVA plot represent the statistical distribution of impedance vectors for a population, with the size and orientation of the ellipse indicating the variability and correlation between resistance and reactance across individuals (28) (see *Materials and Methods* for more details). However, existing BIVA results are based on resistance and reactance measured from hands to feet or wrists to ankles, which limits its practicality for continuous ambulatory monitoring. The potential of using localized BIVA for the continuous assessment of WBH has never been explored due to the lack of suitable wearable sensors.

Recent advances in dry, skin-soft, and skin-conformable epidermal electronics, a.k.a., e-tattoos (31, 32), have spurred the development of wearable Bio-Z sensors but mainly for the purpose of measuring skin hydration (33–38). Skin-conformable gold nanomembranes (34) and highly breathable nanomesh electrodes (39) have been used to detect skin hydration levels without altering skin functions. Despite their effectiveness, their bipolar measurement configuration and small electrode spacing restricted them to tracking the hydration of superficial skin layers. Microfluidic-based wearable biosensors have been reported to detect sweat loss and have garnered significant attention (40, 41). However, these sweat sensors have not been shown to monitor whole-body dehydration resulting from conditions such as vomiting or diarrhea.

Here, we introduce a wireless and wearable WBH sensor based on tetrapolar Bio-Z sensing with strategically placed electrodes across the arm (Fig. 1*D*). Two pairs of temporary tattoo-like, skin-conformable dry electrodes for high-frequency AC injection and voltage sensing allow cross-arm Bio-Z measurement in the transmission mode (Fig. 1*E*). The effects of electrode configuration including electrode spacing d are systematically studied by finite element analysis (FEA) and an optimal configuration is determined. The measured resistance and reactance are wirelessly transmitted to a smartphone via Bluetooth Low Energy (BLE) in real time. To avoid complications in Bio-Z detection caused by temperature or motion, we designed a diuretic-induced dehydration protocol that requires minimal movements and temperature fluctuation in an indoor setting (Fig. 1 *F*, *Top*). The cross-arm Bio-Z and BIVA obtained by our sensor closely match the whole-body Bio-Z and BIVA measured by a commercial impedance analyzer connected to conventional gel electrodes. To demonstrate the wearability and continuous sensing capability of our wearable WBH sensor, we also conducted a 24-h continuous measurement under free-living conditions (Fig. 1 *F*, *Bottom*). We demonstrate the feasibility and effectiveness of a Bio-Z sensor featuring a cross-arm sensing configuration for continuous WBH assessment. This new capability has significant potential to improve awareness of WBH and facilitate proactive health management in everyday life or for high-risk and high-activity populations.

Results

Effects of Electrode Configuration on Human Brachium. Bio-Z sensing for WBH necessitates the strategic placement of the two pairs of electrodes for current injection and voltage sensing purposes. These electrodes serve the function of stimulating the tissue by applying a high-frequency AC and measuring the resultant potential, which fluctuates in response to impedance variations within the underlying tissue. When deployed around the brachium, the measured Bio-Z exhibits sensitivity to various factors such as changes in body fluids (e.g., blood flow, tissue hydration) and motion. To develop a hydration sensor that has enough sensitivity to these fluid shifts, FEA were conducted to determine: 1) the optimal sensing configuration and 2) the best current-to-voltage electrode spacing. The results of these FEA guided the design and placement of the device.

Previous applications of tetrapolar Bio-Z sensing typically adopt an arrangement where all electrodes are positioned linearly along various arteries of the body (e.g., wrist, ankle, neck), with the outer electrodes serving for current injection. This configuration is effective in capturing temporal arterial activities (for example, pulse transit time) to obtain cuffless blood pressure

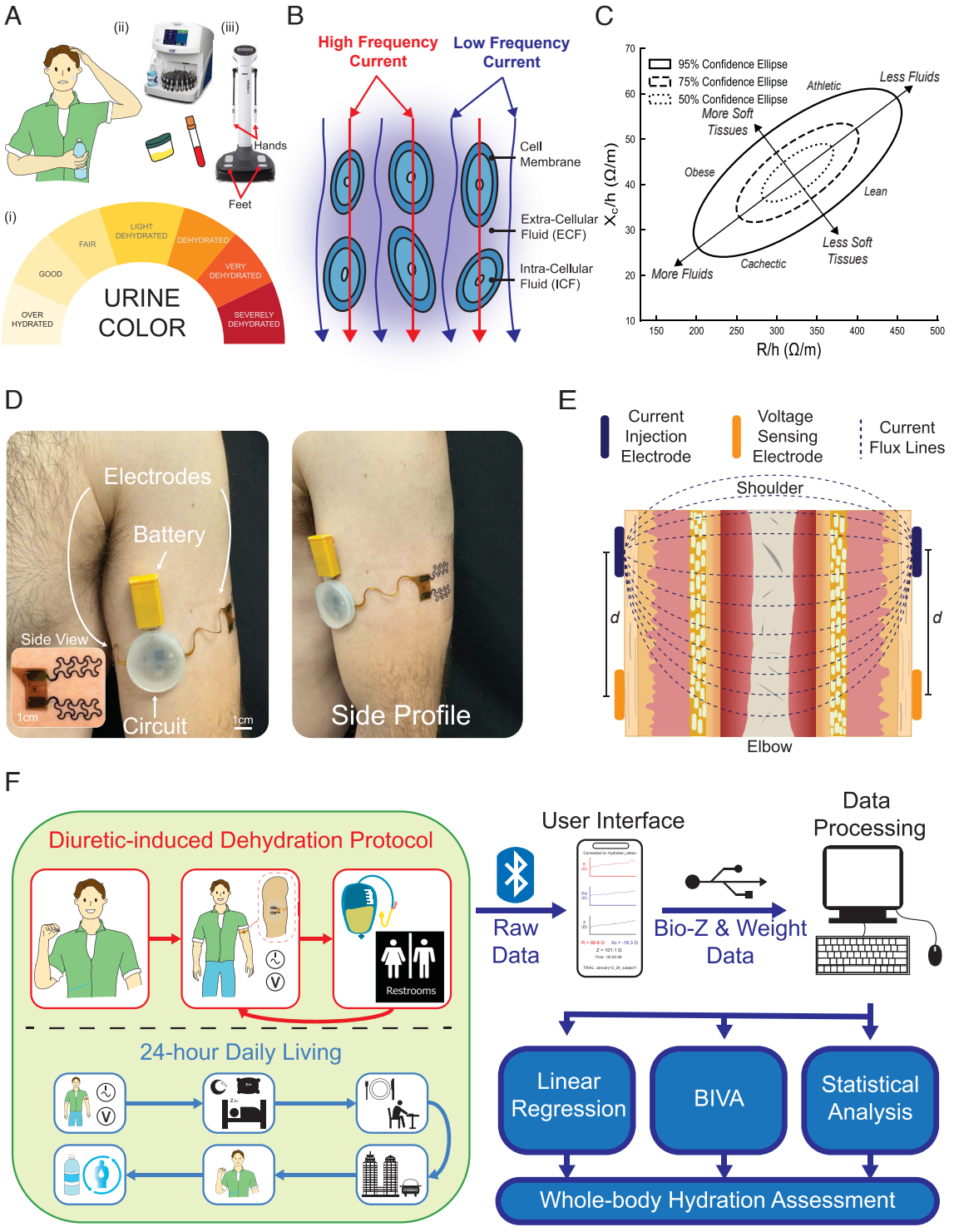

Fig. 1. Overview of our wireless wearable bioimpedance (Bio-Z) sensor for continuous assessment of whole-body hydration (WBH). (*A*) Established methods for WBH assessment: i) urine color chart; ii) blood or urine lab tests; iii) whole-body Bio-Z analysis machine. (*B*) High frequency AC can flow through extracellular fluid (ECF) whereas low frequency AC flows through intracellular fluid (ICF). (*C*) Established whole-body bioelectrical impedance vector analysis (BIVA) where reactance (X_c) normalized by body height (h) is plotted vs. resistance (R) normalized by body height (h). Ellipses indicate different identified hydration states and body compositions based on the BIVA of a population of 15,903. (*D*) Our wireless Bio-Z sensor, designed to be worn on the upper arm, features electrodes arranged diametrically across the arm in a tetrapolar configuration. The *Lower Left Inset* shows one side of the arm with two skin-conformed e-tattoo electrodes. The *Left* image shows the front-view of the device on a relaxed arm while the *Right* image shows the side profile of the device. (*E*) Schematic illustration of tetrapolar Bio-Z sensing on the upper arm, where the longitudinal distance between the current and voltage electrode d is a key parameter. (*F*) An overview for the two human test protocols in this work and the data flow.

(19, 42). However, in our study, the primary focus is on capturing deep tissue Bio-Z that can sufficiently represent the WBH. Therefore, the "cross-arm configuration" is proposed, in which the two current injection electrodes are placed on the opposite side of the brachium along with the two voltage sensing electrodes, as illustrated in Fig. 2*A*. As a result, on each side

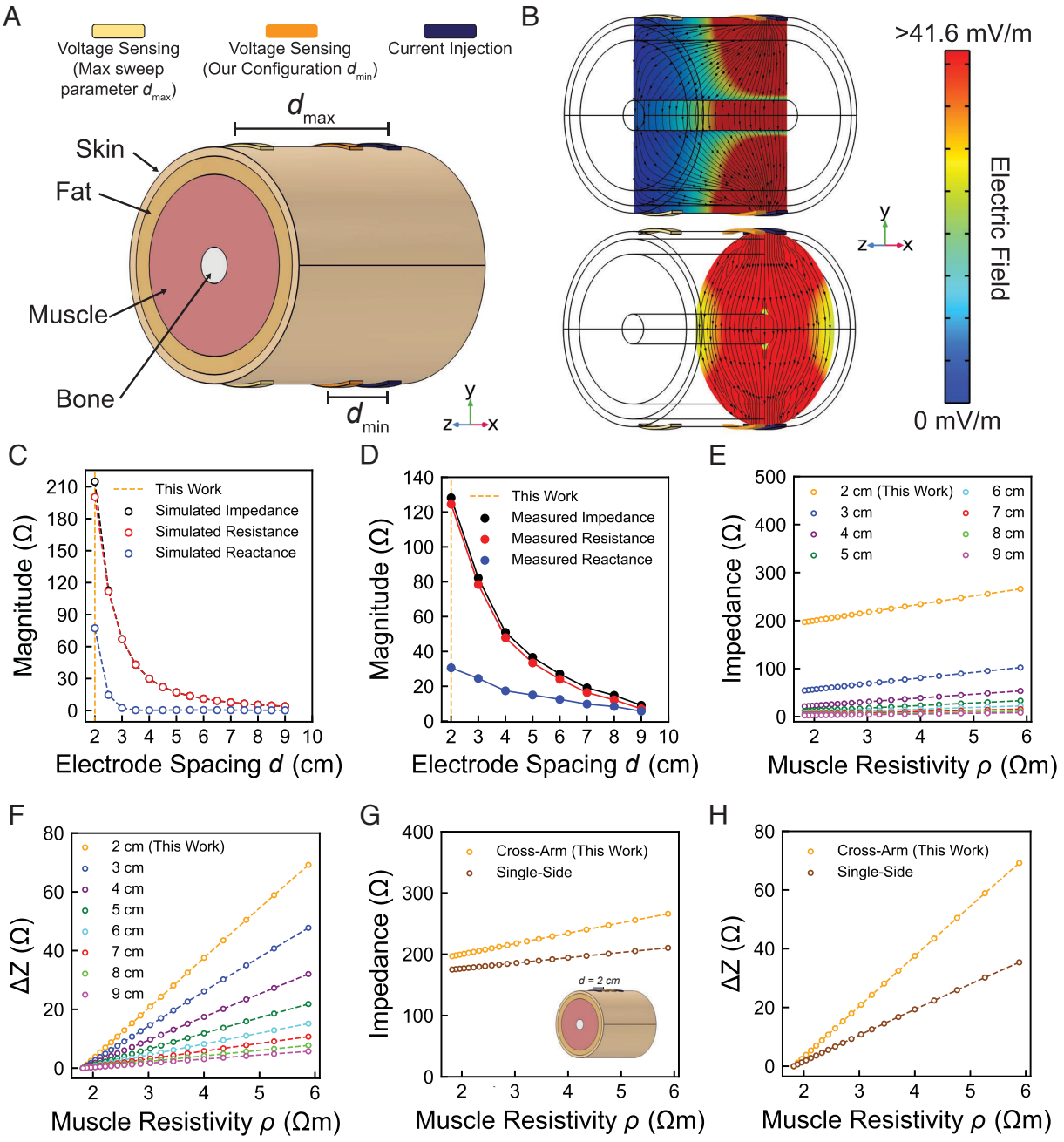

Fig. 2. Finite element analyses (FEA) and experimental measurements of brachium Bio-Z. (*A*) Three-dimensional (3D) FEA model of a tetrapolar electrode arrangement across the brachium, which is composed of four different tissue layers (i.e., skin, fat, muscle, bone) with well-defined electrical characteristics. (*B*) Two orthogonal cross-sectional views (XY and YZ planes) of the simulated contours of the electric field under cross-arm tetrapolar electrode placements as illustrated in (*A*). (*C*) Simulated and (*D*) experimentally measured resistance, reactance, and impedance as a function of electrode spacing d. (*E*) Simulated total impedance and (*F*) change in impedance as a function of muscle resistivity ρ for varying electrode spacings. (*G*) Simulated impedance and (*H*) change in impedance as a function of muscle resistivity ρ comparing cross-arm to single-sided electrode placements with $d = 2cm$. The *Inset* in (*G*) illustrates the single-sided sensing configuration.

of the brachium, a current electrode and a voltage electrode are placed side by side. The longitudinal distance between the two, d, becomes an important parameter that affects the Bio-Z measurement. To perform FEA, a four-layer tissue model of the brachium was established (Fig. 2*A*). From exterior to interior, the volume fractions of the skin, fat, muscle, and bone are 0.148, 0.260, 0.568, and 0.024, respectively (43). The frequency-dependent electrical properties of each type of tissue were derived from the Cole–Cole equations (44) and are tabulated in *SI Appendix*, Table S1. Note that the electrical conductivity of the skin is three orders of magnitude lower than that of the muscle. The current-voltage electrode distance d was varied in the simulation to elucidate its effects on tetrapolar Bio-Z sensing. In our FEA, 100 μA of AC at a frequency of 40 kHz was employed. Electrical simulations were conducted using the AC/DC physics module of COMSOL Multiphysics v6.1 and the details are provided in *Materials and Methods*.

Fig. 2*B* plots the electric field contour of two orthogonal (longitudinal and transverse) cross sections of the model. Notably, the cross-arm configuration forces the current to flow through the entire arm, which can be called the "transmission mode," whereas the current passes predominantly through the top half

in the single-sided electrode arrangement (*SI Appendix*, Fig. S1), which can be called the "reflection mode." In both cases, the FEA indicate that current penetrates through the muscle as a result of the deep-tissue penetrating capabilities of high frequency AC. However, because of its limited penetration depth, the reflection mode is not as effective as the transmission mode in capturing hydration-dependent Bio-Z. Given the high water content and high conductivity of muscles, reliable Bio-Z-based WBH assessment requires the AC to pass through adequate muscle mass. As a result, even in the transmission mode, the distance between the current injection electrode and the voltage sensing electrode, d, plays a pivotal role. As expected, the electric field is the highest right beneath the injection sites and quickly decays with increasing distance (Fig. 2*B*). As a result, when the voltage sensing electrodes are placed too far away from the current injection electrodes, the measured Bio-Z is expected to be less sensitive to hydration changes. Fig. 2*C* plots the simulated Bio-Z amplitude (black), resistance (red), and reactance (blue) as functions of current-voltage electrode distance d. It is apparent that all three measurements increase with decreasing d, which is due to shorter and more constricted current paths. The FEA findings were confirmed by tetrapolar measurements on a human arm using commercial wet-gel electrodes (Red Dot Electrodes, 3M) with varying electrode spacings (Fig. 2*D*). In spite of numerical mismatches due to the simplified FEA model, the measured trends closely resembled those of the simulation. In both cases, the Bio-Z are found to be dominated by resistance as the fluid-rich muscle tissue is fairly conductive. With the experimental validation of our FEA, we further utilized the FEA to acquire more insights into the electrode arrangements.

We first simulated the dehydration process by increasing the electrical resistivity (ρ) of muscle tissue, based on the well-established negative correlation between electrical resistivity and body water content (45), and given that fat-free muscle tissue is composed of approximately 75% water (46). Additional simulations were conducted by varying the electrical resistivity of the skin, but only minor changes in Bio-Z were observed. This outcome was expected, as the skin constitutes a small fraction of the mass and the tetrapolar configuration minimizes its influence. Fig. 2 *E* and *F* indicate how the absolute and change in Bio-Z vary with increasing muscle resistivity at eight different d values between 2 and 9 cm. The upper limit of this range corresponds to the average brachium length of an adult male. Notably, the smallest electrode spacing demonstrates the highest sensitivity to tissue dehydration. Taking $d = 2cm$, we further compared the impedance change with ρ between transmission vs. reflection modes (Fig. 2 *G* and *H*) and confirmed the expectation that the transmission mode enabled by the cross-arm electrode arrangement is more sensitive to muscle dehydration. Based on Fig. 2, it can be concluded that the optimal device configuration should include the minimum feasible separation between the current injection and voltage sensing electrodes, arranged in a cross-arm pattern. Therefore, we designed our Bio-Z-based WBH sensor to operate in transmission mode with a 2-cm electrode spacing.

Device Design and Bioimpedance Data Acquisition. After establishing the electrode arrangement, we designed a flexible printed circuit (FPC) to capture Bio-Z signals from the arm and transmit the collected data wirelessly, allowing mobile and continuous Bio-Z recording. Fig. 3*A* offers a block diagram of the FPC. The Bio-Z analog front end (AFE) (MAX30002, Maxim Integrated) serves as a single-channel Bio-Z readout (which is also schematically depicted in *SI Appendix*, Fig. S2). It is connected to the central processing unit (CPU) nRF52832 (Nordic Semiconductor, USA) with integrated BLE. A 3.7 V 40 mAh lithium polymer (LiPo) battery supplies power to the circuit through a 1.8 V linear low-dropout regulator (NCP161, onsemi). The physical layout of the FPC and e-tattoo electrodes is illustrated in Fig. 3*B*. All active components are placed on a central island with a diameter of 2.4 cm, strategically placed to rest on the bicep head. From this island, a short extension provides a convenient plug-and-play connection through an easy-on FPC port (Molex, USA) soldered to a LiPo battery. Two serpentine-shaped stretchable interconnects extend from the island to provide stretchability when wrapped around the arm. The end of each serpentine interconnect has two exposed terminal pads for electrode attachment. Instead of using commercial silver–silver chloride (Ag/AgCl) gel electrodes which can dehydrate over time and detach during muscle flexion, four filamentary serpentine-shaped stretchable electrodes were made of 50-μm-thin graphite polyurethane (GPU, Mineral Seal Corporation) sheets using the cut-and-paste method (37). Wireless e-tattoos with filamentary serpentine GPU-based dry electrodes have been worn for more than 24 h without signal degradation (47). They can be affixed to the skin through 3M Tegaderm tapes and connect to the terminals through anisotropic conductive films (ACF). The ACF enables simple attachment and removal between the FPC and the double-sided conductive GPU electrodes, allowing the electrodes to be disposable while the FPC remains reusable. More details of the fabrication and integration of the sensor hardware are available in *Materials and Methods*. The entire system, including the battery, weighs only 4 g. This layout design imparts stretchability to fit different arm sizes, minimizes the number of interconnects, and promotes long-term operation and reuse of the FPC.

The device uses an AC current of 100 μA at 40 kHz to comply with the safety standards for current injection (48) and previous BIVA performed at 50 kHz (24, 26). A sampling frequency of 0.2 Hz is used as human hydration does not change rapidly, which also helps reduce power consumption. Fig. 3*C* displays the sensor's average power draw during operation, which is only 0.879 mA.

The skin–electrode interface (i.e., "contact") impedance is a critical factor for Bio-Z measurements. Fig. 3*D* compares the measured contact impedance of dry GPU electrodes (red) with commercial wet gel electrodes (blue) at 40 kHz: 4.1 KΩ and 0.39 KΩ, respectively. For an injection current of 100 μA, both impedance levels are well within the system limit (i.e., 1.8 V).

Fig. 3*E* illustrates that the resistance of the FPC's interconnect remains almost unchanged up to a tensile strain of 45%. The central island of the FPC is encapsulated by a biocompatible and electrically insulating silicone elastomer (Ecoflex 00-30, Smooth-On, Inc.) with a Young's modulus comparable to that of the human dermis (31). It prevents the direct contact between the wearer and active electronic components. Furthermore, the hydrophobic properties of the silicone elastomer create a moisture barrier, protecting the FPC against possible sweat corrosion. The encapsulated device can withstand bending, twisting, and stretching (Fig. 3*F*), demonstrating its suitability as a wearable device on the highly deformable human brachium. Fig. 3*G* shows the overall appearance of the device during tricep extension and bicep flexion, demonstrating the mechanical robustness and the wearability of the device. The stability of the Bio-Z measurement was additionally tested under muscle contractions and movement. *SI Appendix*, Fig. S3 presents arm Bio-Z data collected for 45 min during which a single participant engaged

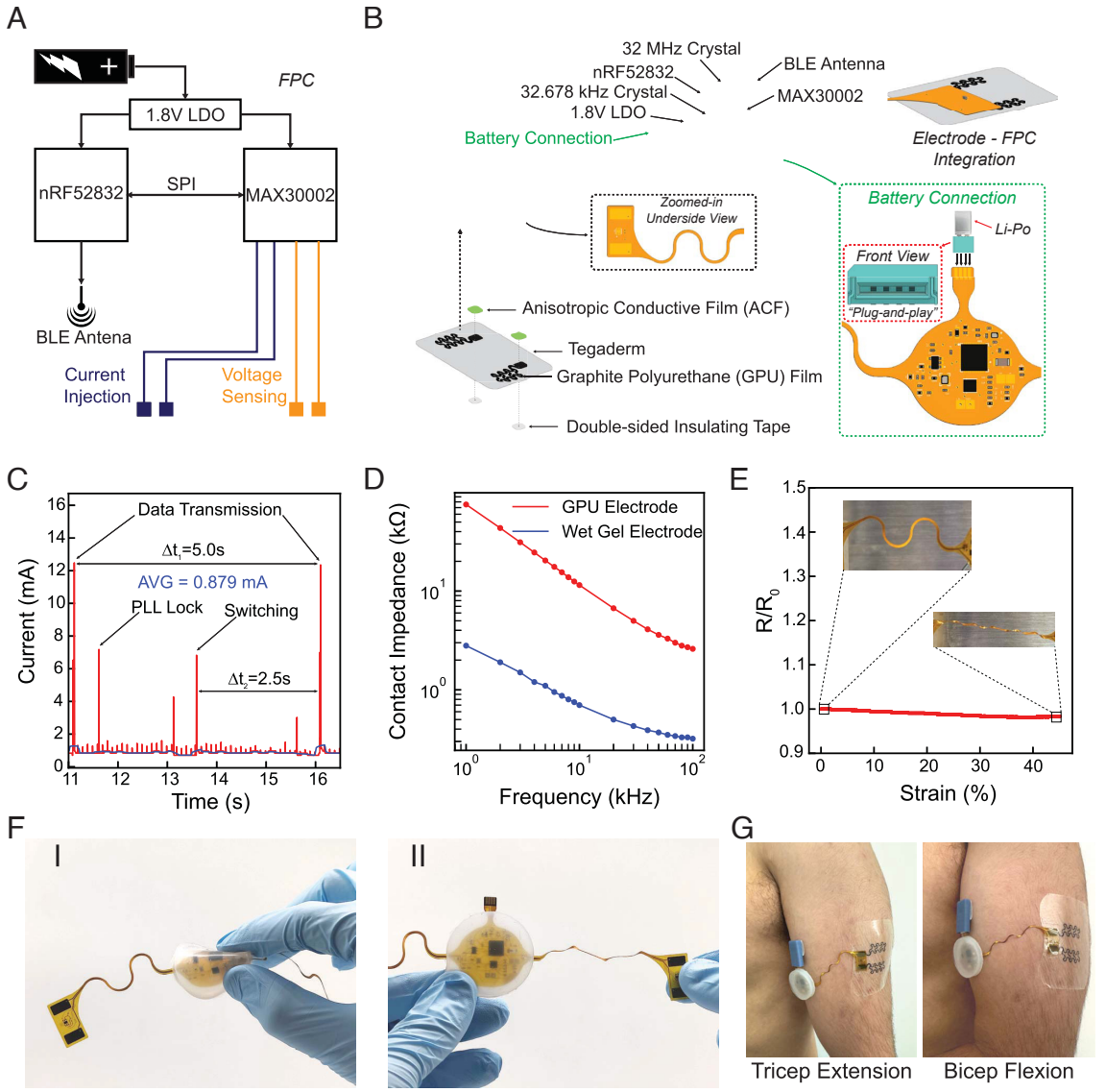

Fig. 3. Device design and characterization. (*A*) Block diagram of the FPC and battery. (*B*) Physical layout of the FPC, battery, and tattoo electrodes. (*C*) The average current draw of the device is 0.879 mA. Current draw peaks during data transmission at a rate of 0.2 Hz. (*D*) Contact impedance with the skin as a function of frequency for graphite polyurethane (GPU) dry electrodes (red) and wet gel electrodes (blue). (*E*) Resistance-strain curve for the serpentine interconnects on the FPC. (*F*) FPC with Ecoflex encased circuit island under I) bending and serpentine interconnects under II) stretching and twisting. (*G*) Device worn on the brachium under various muscle contractions showcasing mechanical robustness and wearability.

in muscle contraction exercises. These exercises included periods of medium and full bicep flexion interspersed with rest intervals. Medium muscle flexion required the participant to maintain their arm at a 45°angle relative to a flat surface, while full muscle flexion was carried out without constraining the angle of the arm. Each flexion period lasted five minutes and consisted of alternating 15-s intervals of flexion and rest. This process was repeated twice. The average percent Bio-Z deviation from baseline was 3.3% during medium muscle flexion of the bicep and 9.8% during flexion of the entire muscle. Notably, the signal consistently returned to its baseline after each exercise, underscoring the robustness and repeatability of the wearable Bio-Z sensor.

Diuretic-Induced Dehydration Experiments. To evaluate the capabilities of the WBH sensor, a diuretic-induced dehydration experiment was conducted in the lab, following the protocol shown in Fig. 4*A*. This protocol aims to prevent Bio-Z distortion caused by movement or changes in skin temperature (49, 50). All participants were asked to have a regular breakfast and be well hydrated before coming to the lab. The tests began with preparing the participant's upper arm by gently scrubbing it with an exfoliating gel, followed by cleaning it with a saline wipe and then drying it with a task wipe. The device was attached to the left upper arm as all participants were right-handed. During data collection, participants were allowed to perform relatively static tasks, such as using a phone, laptop, or reading with their dominant hand.

After wearing the sensors, participants were given 40 mg of Furosemide, an oral loop diuretic, to promote fluid loss. Furosemide works by preventing sodium and chloride reabsorption in the kidneys, which reduces water reabsorption and increases urine output. This leads to a significant loss of both solutes and water, causing dehydration with little change in ECF osmolality. This kind of dehydration, called isotonic dehydration, is similar to that caused by conditions such as diarrhea and vomiting (17).

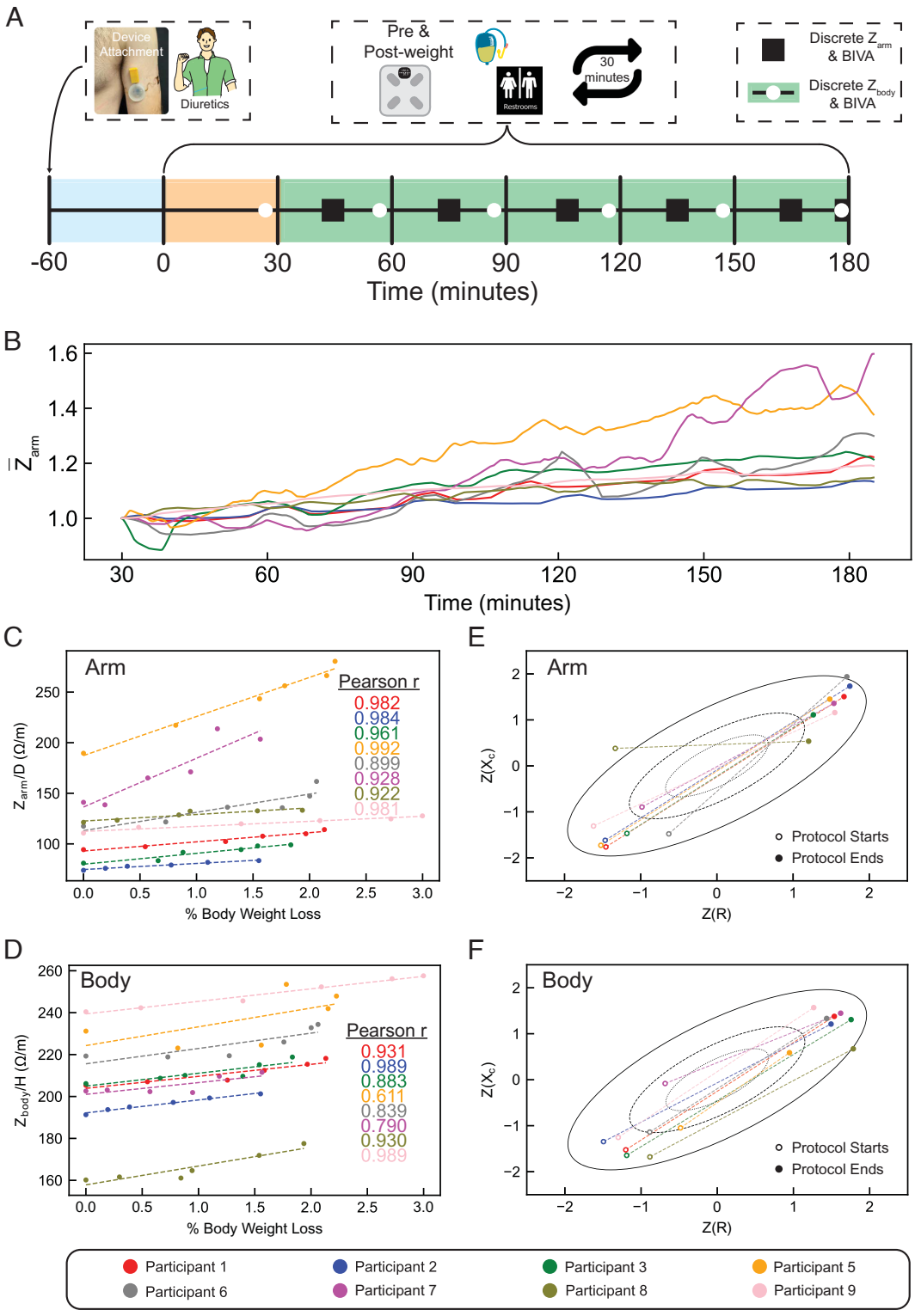

Fig. 4. Diuretic-induced dehydration experiment conducted with nine participants. (*A*) Experimental protocol. Blue section [−60 min, 0] represents no data collection and only for the diuretic to take effect, orange section [0, 30 min] represents the time given for the dry GPU electrodes to stabilize its contact impedance with the skin, and green sections [30 min, 180 min] represent useful Bio-Z data. Urination occurred every 30 min and body weight was taken before and after each urination. Black squares represent the 5-min windows for average arm Bio-Z calculation, and white dots represent the body weight measurements right before each urination. (*B*) Continuous arm Bio-Z measured by the wearable sensor normalized by initial Bio-Z values over time. Both (*C*) arm-diameter-normalized arm Bio-Z and (*D*) height-normalized whole-body Bio-Z (measured by LCR meter) show strong linear correlation with percent body weight loss. (*E*) Arm and (*F*) whole-body BIVA plots.

Data collection began 60 min after the device was attached and furosemide was taken, allowing the diuretic to take effect. Data were collected for three hours, with the first 30 min accounting for electrode settling effects, and during which time participants urinated every 30 min. Participants were restricted from fluid and food intake during the data collection period. Body weight

was measured before and after each urination using bath scales to quantify changes in body water. Body weight change is a good indicator of body water loss because during the three-hour dehydration experiment, there was no food or fluid intake and only minimal changes in body glycogen and fat occurred, which were evenly balanced by water produced from substrate oxidation (51, 52).

Numerous studies have used whole-body Bio-Z to evaluate WBH (24, 26–30). Thus, to enable comparison with existing studies and to establish a baseline for comparing Bio-Z measurements from the arm to that of the whole body, participants also had whole-body Bio-Z measurements collected approximately 5 min before each urination event, as indicated by the white dots in Fig. 4*A*. These were performed using a high-precision LCR meter (E4980AL, Keysight Technologies) connected to commercial gel electrodes attached to the wrists and ankles of the participants.

Bioimpedance and WBH Analysis. Arm Bio-Z, whole-body Bio-Z, and body weight were collected from a group of nine healthy participants following the predefined experimental protocol. The group included eight males and one female, ages 26.3 ± 3.3 y, with an average weight of 75.7 ± 12.4 kg, height of 179.8 ± 6.3 cm, and body mass index (BMI) of 23.3 ± 3.1. Throughout the diuretic-induced dehydration study, participants experienced an average weight loss of 1.65 ± 0.30 kg (or 3.64 ± 0.66 lbs), equating to a 2.30 ± 0.40% reduction in body weight. Real-time arm resistance R and reactance X_c were continuously recorded using our wearable sensor. The Bio-Z is calculated as the magnitude of the $R - X_c$ vector

$$Z = \sqrt{R^2 + X_c^2} \quad [1]$$

For data comparison between participants, the initial arm Bio-Z Z_0 (measured at t = 30 min) was used as a baseline for normalization in Fig. 4*B*.

$$\overline{Z} = \frac{Z}{Z_0} \quad [2]$$

This normalization allowed analysis of common trends in arm Bio-Z changes, which consistently increased during the study period, indicating alterations in hydration status. Fig. 4*B* plots the time-dependent changes in the normalized arm Bio-Z, $\overline{Z}_{\text{arm}}$, for eight participants, excluding one male participant due to insufficient weight loss and data quality issues possibly due to an unsecured ACF connection between the GPU electrodes and the FPC. The remaining data were postprocessed with median and mean filtering to remove noise and smooth trends, particularly during urination events. Note that motion artifacts—even during significant activities such as urination—contribute far less than the observed 25% dehydration-induced impedance change, confirming the robustness of the arm Bio-Z WBH measurement against typical daily movements.

To directly compare continuously collected Bio-Z data with discrete body weight measurements, Bio-Z data between two urination events were averaged over 5-min intervals to produce a single Bio-Z value for comparison, shown as black squares in Fig. 4*A*. Each Bio-Z value was matched to the body weight measurement recorded right before each urination event. For example, the Bio-Z value at the 45-min mark was averaged from data between 42.5 and 47.5 min and compared to the body weight measurement at t = 30 min. Fig. 4*C* plots the arm Bio-Z normalized by arm diameter against percent body weight loss for each of the eight participants. All participants exhibited strong positive linear correlations, shown by Pearson's correlation coefficients r. In general, these coefficients ranged from 0.899 to 0.992, with an average of 0.956 ± 0.033. The strong correlation between the observed increase in arm Bio-Z and the percent body weight loss suggests that arm Bio-Z can effectively serve as a surrogate for WBH. By combining the FEA results in Fig. 2, which show a linear relationship between arm Bio-Z and muscle resistivity, with the experimental results in Fig. 4, which demonstrate a linear relationship between arm Bio-Z and WBH, we confirm the previously established linear relationship between muscle electrical resistivity and body water content (45). This offers a practical method for mobile and continuous WBH assessment. Note that recent wearable Bio-Z sensors with linearly arranged electrodes on the human back and operating in reflection mode showed much weaker correlation ($r < 0.8$) with body fluid loss (20), highlighting the importance of the transmission mode enabled by the FEA-guided cross-arm tetrapolar Bio-Z sensing configuration.

Fig. 4*D* shows the relationship between height-normalized whole-body Bio-Z and percent body weight loss for each participant. Like Fig. 4*C*, a positive linear correlation was observed for all participants. The smaller variation in the slopes of height-normalized whole-body Bio-Z (Fig. 4*D*) compared to arm-diameter-normalized arm Bio-Z (Fig. 4*C*) suggests that height provides a more consistent normalization across individuals. In contrast, arm diameter normalization is more sensitive to anatomical differences. However, compared to Fig. 4*C*, Pearson's correlation coefficients in Fig. 4*D* varied more widely from 0.611 to 0.989 and the overall correlation for the group was 0.870 ± 0.117. This increased variability, compared to arm Bio-Z, may result from: 1) whole-body Bio-Z data being more affected by fluid shifts occurring in the gastrointestinal and other body areas (e.g., cardiac blood flow); 2) whole-body Bio-Z being more responsive to posture changes, despite participants being instructed to sit upright. Consequently, despite the widespread use of whole-body Bio-Z for WBH assessment, arm Bio-Z appears to be a superior option.

BIVA. Although Bio-Z is effective in correlating with body water loss in our experiment, BIVA introduced in Fig. 1*C* provides more nuanced insights into WBH and body composition by separating resistance R and reactance X_c. Detailed introduction to BIVA can be found in *BIVA* in *Materials and Methods*.

Applying the standard z-transform to each participant's arm Bio-Z data, their vector displacements can be plotted in one chart relative to the healthy reference population. The z-transform converts the resistance and reactance data into z scores to preserve the analytical interpretation (17). Fig. 4 *E* and *F* plot the measured arm and body BIVA vectors for each participant, with open and solid markers indicating the start and end of the protocol, respectively. Eight out of the total eight body BIVA vectors and seven out of the total eight arm BIVA vectors point to the upper right along the long axis, which is consistent with trends associated with body water loss reported in the literature based only on whole-body BIVA (26, 53). A possible reason for the abnormal arm BIVA of Participant 8 can be attributed to a minimal change in arm reactance throughout the protocol, which itself may be due to physiological factors or a poor electrode–FPC interface. Other than Participant 8, the comparable arm and body BIVA suggests that BIVA can be extended from the whole body to a local segment, e.g., the

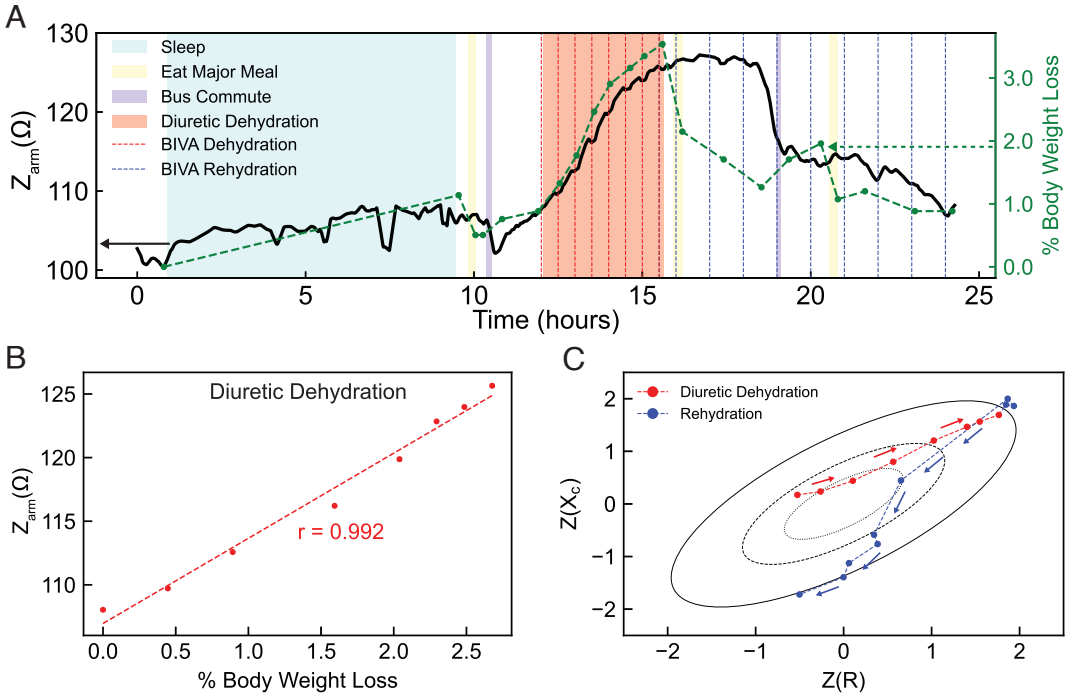

Fig. 5. Continuous 24-h ambulatory experiment testing the wearability and efficacy of the wireless sensor. (*A*) Bio-Z measured by the sensor (black curve) and percent body weight loss (green dashed curve) during the 24-h experiment which includes a diuretic-induced dehydration session (orange shaded period). Vertical dashed lines correspond to the data points in *B* and *C*. (*B*) Arm Bio-Z during the diuretic dehydration session shows a strong linear correlation with the percent body weight loss. (*C*) BIVA plot for the dehydration (red) and rehydration (blue) periods. Note that the red arrows indicate a change toward a more dehydrated state while the blue arrows indicate a change toward a more hydrated state.

brachium, which is possible to measure using a wearable device. Moreover, since arm resistance and reactance are continuously measurable by the wearable sensor and BIVA does not necessitate body weight assessment, vectors can be plotted for any given time point, offering a temporally relevant representation of hydration status. *SI Appendix*, Fig. S4 underscores this benefit by depicting arm BIVA and whole-body BIVA at different stages of the experimental protocol, demonstrating vector displacement toward an increasingly dehydrated state over time.

Another important implication of the BIVA plot is that the location of each individual marker relative to the reference ellipses indicates the hydration status of the person at that moment. For example, markers in the third quadrant indicate fluid overload and markers in the first quadrant indicate a dehydrated state. Moreover, the length of the BIVA vector from the starting marker to the end marker is known to be inversely related to the loss of TBW (54), with shorter vectors indicating minor fluid loss/gain while longer vectors suggesting a larger shift in hydration status. Previous studies have attempted to leverage vector lengths to estimate hydration status (26). In this study, vector lengths were computed utilizing the Euclidean distance formula:

$$d = \sqrt{(x_2 - x_1)^2 + (y_2 - y_1)^2}, \quad [3]$$

where (x_1, y_1) and (x_2, y_2) represent the BIVA coordinates at the starting and the current times, respectively. *SI Appendix*, Fig. S5 illustrates how vector length correlates with the percentage of body weight loss for each participant, calculated from the vectors shown in *SI Appendix*, Fig. S4 using the Euclidean distance formula. The arm BIVA vector lengths and the percent body weight loss demonstrate a robust positive linear correlation with a Pearson's correlation coefficient of 0.93 ± 0.07 (*SI Appendix*, Fig. S5*A*). In contrast, correlations between whole-body BIVA vector length and percent body weight loss are weaker with greater variability (0.76 ± 0.27 as in *SI Appendix*, Fig. S5*B*). This higher variability is consistent with the total Bio-Z to percent body weight loss correlations comparing Fig. 4 *C* and *D*, which can be attributed to the factors previously discussed.

To demonstrate measurement repeatability on the same subject, *SI Appendix*, Fig. S6 presents data from a single participant who completed three independent trials of the diuretic-induced dehydration protocol. Although offsets in absolute values are notable (*SI Appendix*, Fig. S6*A*), the normalized changes in arm Bio-Z remain consistent across all trials (*SI Appendix*, Fig. S6*B*), and in each case, Bio-Z changes show a strong correlation with body water loss (*SI Appendix*, Fig. S6*C*). Furthermore, the vectorial displacements in the BIVA plot consistently align with the long axis and are highly reproducible across the three trials (*SI Appendix*, Fig. S6*D*). These results confirm the repeatability of our arm-worn sensor in measuring Bio-Z and BIVA for monitoring body dehydration.

Additional experiments were carried out to illustrate why the arrangement and anatomical site of the electrodes are critical for meaningful BIVA. In the unilateral arrangement of *SI Appendix*, Fig. S7, all four electrodes reside on one side of the upper arm, so the current loops back superficially (reflection mode). Although resistance still increases with dehydration, the reactance hardly changes, causing vectors to slide along the minor ellipse axis and obscuring hydration trends. In *SI Appendix*, Fig. S8, wrist-level cross-arm placement suffers even more: the narrow bone-and-tendon column offers little conductive muscle, and frequent hand motions introduce spikes, so the capacitive component is nearly lost, and BIVA vectors collapse toward the origin. Together, these results confirm that the deep muscle-traversing current paths provided by our cross-arm configuration at the brachium, which has adequate muscle mass to represent WBH, are essential

for balanced resistance-reactance changes and a reliable and interpretable BIVA trajectory. As a result, we always adopt the placement of the device shown in Fig. 1*D*.

24-h Ambulatory Monitoring of WBH. In addition to the diuretic-induced dehydration experiment in the lab, a 24-h ambulatory study was conducted on a single human participant (male, age 26). The primary objective of this experiment was to demonstrate the long-term monitoring capabilities of the sensor, evaluating its efficacy in monitoring hydration status continuously during routine daily activities. Furthermore, the study sought to evaluate the reliability and wearability of the device during sleep and other daily tasks, as well as to determine the sensor's ability to track the rehydration process after dehydration.

Fig. 5*A* shows the Bio-Z data collected in the 24-h ambulatory experiment. Body weight was measured using commercial bathroom scales after major activities or when the participant urinated, ate, or drank. Activities such as sleep, bus travel, and major meals are highlighted using shades in the graph. A diuretic-induced dehydration protocol, allowing no fluid or food, was included to represent medication use. Otherwise, diet and fluid intake were not restricted. Data were collected throughout rehydration and food intake to provide relevant information. During the ambulatory dehydration test (orange-shaded period), Z_{arm} still closely tracked the percent body weight loss similar to the lab tests. However, after the dehydration test ended, the body weight quickly recovered after a major meal, while Z_{arm} continued to increase mildly after drink and food intake and only started a significant decrease about three hours later. This discrepancy can be attributed to the contribution of solid foods to body weight and delayed tissue rehydration after fluid intake. Eight hours after the dehydration experiment ended, body weight loss and arm Bio-Z converged and almost returned to their pre-dehydration baseline values, indicating that long-term Bio-Z can provide a reversible measure of WBH despite its lag in tracking rapid body weight increases due to fluid and food intake. This reminds us that body weight loss is no longer a reliable measure of WBH right after meals and that is why our lab dehydration experiment as shown in Fig. 4 excluded meals and fluid. Although short-term fluctuations of the arm Bio-Z in the range of ± 2 to 3 ohms can be observed during activities such as meals and bus trips, they are relatively minor compared to the $\sim$20 ohm change observed during significant dehydration. This experiment demonstrates the sensor's ability to monitor major hydration changes effectively over time. The red and blue vertical dashed lines in the figure indicate the time stamps for the red and blue data points in Fig. 5 *B* and *C*.

As shown in Fig. 5*B*, there is a strong positive linear correlation between arm Bio-Z and percent body weight loss during the diuretic dehydration experiment, matching the trends in Fig. 4*C*. Fig. 5*C* displays the BIVA plot for the dehydration (red) and rehydration (blue) periods. Vector displacements show a shift from hydrated to dehydrated states due to diuretic intake, and back to a hydrated state after rehydration and food intake.

Three weeks later, the same participant joined a second 24-h session wearing a rigid Bio-Z measuring PCB connected to commercial gel electrodes through cables. *SI Appendix*, Fig. S9 shows that these results align closely with those in Fig. 5. However, the arm Bio-Z data acquired by the rigid PCB and gel electrodes show more fluctuations than those acquired by the FPC and tattoo electrodes. The participant also noted gel electrode delamination after 20 h, indicating unstable sensor performance with prolonged use. These observations highlight the benefits of soft FPC and tattoo electrodes for comfortable and reliable ambulatory sensing.

To eliminate the effects of solid food on rehydration, a 6-h study—comprising three hours of dehydration followed by three hours of fluid-only rehydration—was conducted with two participants. The results are shown in *SI Appendix*, Fig. S10. During the rehydration phase, participants consumed a total of three liters of sports drink (Pedialyte) at timed intervals marked by vertical dashed lines, without consuming any solid food. Notably, a similar lag effect to that seen in Fig. 5 is observed: Arm Bio-Z continues to rise mildly beyond the end of the dehydration phase and throughout rehydration, eventually plateauing without a clear return to baseline within the observation window. Compared to Fig. 5*A*, *SI Appendix*, Fig. S10 suggests that fluid-only rehydration does not reduce the lag time. One possible explanation is that during diuretic-induced dehydration, fluid is lost relatively uniformly from both blood plasma and interstitial compartments, enabling the local Bio-Z signal to track water loss almost immediately. In contrast, during rehydration, fluid absorption, and redistribution—particularly into the interstitial space—requires more time, resulting in a delay between body weight recovery and local tissue hydration as reflected by Bio-Z. This highlights one key advantage of Bio-Z over simple weight measurements, as Bio-Z directly measures the electrical properties of the tissue that reflect the actual hydration state rather than just the changes in body mass.

Discussion

The lack of wearable technology for real-time, continuous assessment of WBH is a long-standing unmet need for diagnostics and occupational health management. We therefore designed and tested a wireless, arm-worn, Bio-Z sensor capable of noninvasive and ambulatory quantification of WBH. FEA and experimental validations highlight the importance of electrode arrangement on segmental Bio-Z based WBH assessment, emphasizing transmission mode through large muscles and small distance between current injection and voltage sensing electrodes. A pilot study involving nine participants undergoing diuretic-induced dehydration demonstrated the effectiveness of the sensor in real-time WBH tracking, which is even better correlated with percent body weight loss than whole body Bio-Z. The good correlation between arm and whole-body BIVA suggests the potential for extending BIVA from whole-body to local muscles using wearable Bio-Z sensors. In a 24-h ambulatory experiment, the device successfully detected dehydration and rehydration phases. Although arm Bio-Z showed a delayed response compared to immediate body weight recovery after meals, it should be noted that body weight is no longer an accurate surrogate of WBH due to the time delay associated with food digestion and water permeation. In fact, plasma osmolality is a precise but burdensome and impractical laboratory measure of intermittent hydration status (55). Future efforts to monitor heat or exercise-induced dehydration should include 1) utilizing breathable e-tattoos (56) or sweat-wicking wearables (57) to avoid sweat accumulation under tattoo electrodes; and 2) reducing the sensitivity of Bio-Z to motion, as well as changes in skin temperature and blood perfusion. Future studies can also be directed to conducting more extensive tests across a larger cohort of participants and at other segments of the body, such as the forearm and the thigh. It is important to note that the reported arm Bio-Z sensor monitors relative changes in WBH instead of absolute hydration status. A possible approach to overcome this

limitation is to measure the arm Bio-Z of a large population to establish a reference distribution, similar to the extensive body Bio-Z dataset collected from approximately 15,900 adults in NHANES III (1988–1994) (25).

Materials and Methods

BIVA. Compared to BIA, BIVA does not rely on multiple regression equations used to predict fluid volumes and soft tissue composition (FM and FFM). The use of prediction equations for TBW and FFM rely on parameters such as Height^2/Resistance, body weight, age, gender, reactance, and height (58), and additionally rely on the assumption of constant hydration of the FFM (59). Moreover, the models and equations for BIA are typically derived in healthy people and consequently tend to yield inaccurate values of soft tissue composition for individuals with fluid variation. Due to these inherent limitations of BIA, Piccoli et al. introduced the phase-sensitive R-X_C graph method that is based on the analysis of the bivariate distribution of the impedance vector in healthy populations, obese individuals, and individuals suffering from various renal diseases. Unlike BIA, BIVA does not rely on making assumptions about body composition (24).

BIVA is a noninvasive property-based method used to assess body composition and hydration status by measuring the resistance (R) and reactance (X_C) of biological tissue in a similar manner to BIA. Also similar to BIA, BIVA involves the application of electrodes to the arms and legs that pass a current through the body, with the resulting Bio-Z being a composite measure of both resistance, which reflects the opposition to current flow due to ICF and ECF, and reactance, which represents the capacitive properties of cell membranes. However, in contrast to BIA, BIVA considers the R and X_C components separately. The measured values are plotted on the $R - X_C$ graph, providing a graphical representation that allows for the qualitative indication of fluid distribution and body cell mass. The $R - X_C$ graph is constructed using a reference dataset and generates elliptical probability regions to qualitatively indicate hydration status and soft tissue composition. In this study, the elliptical probability regions are generated using the standard reference interval of the NHANES III dataset (25) for healthy young individuals, as provided by Piccoli et al. (60). NHANES III includes whole-body resistance and reactance recordings from approximately 15,900 adults derived from a 50-kHz signal, normalized for height to control for the different stature of individuals. Repeated $R - X_C$ measurements capture the intrasubject variability by leveraging the intersubject variability of data from the reference population.

Previous studies have successfully employed BIVA to assess extracellular and intracellular dehydration (26), monitor body composition during pregnancy (27), discern variations in hydration status and body composition among university athletes (28, 29), as well as monitor the treatment of severe acute malnutrition in children (30).

Finite-Element Analysis of the Human Brachium Bio-Z. Electrical simulations were performed using the AC/DC physics module of the commercial software COMSOL Multiphysics 6.1. A four-layer tissue model, following a cylindrical approximation of the arm, was used to perform the simulations. Experimentally measured values of human tissue properties, at 40 kHz, were used (44), the details of which are summarized in *SI Appendix*, Table S1. Voltage domain probes were assigned to the sensing electrodes to capture the voltage potential as a function of electrode spacing and configuration.

Device Fabrication and Assembly. The electronics are constructed using a double-layer FPC, where a polyimide substrate houses copper tracks on both the top and bottom layers. The FPC design features an island-serpentine configuration, incorporating two islands that house electronics and copper pads for electrode interfacing. These islands are connected to the main board via stretchable serpentine interconnects. Each interconnect comprises the copper tracks required to facilitate the connection between copper surface pads and the electronics. The overall thickness of the FPC, inclusive of circuit elements, measures approximately 1.3 mm. To enhance mechanical stability, the central region of the FPC, which houses the majority of circuit components, is designed using rounded edges. This design facilitates better conformity to human skin and improved resistance against mechanical deformation. In order to ensure safety for use on human participants, the circuit elements were affixed to the FPC using lead-free soldering paste.

Human Participant Recruitment. Inclusion criteria specified enrollment of physically healthy individuals, free from physical disabilities, aged between 18 to 30 y. Exclusion criteria excluded individuals with a documented history of cardiovascular disease, severe dehydration, anuria, or an electrolyte abnormality. Participant selection considered diverse body mass index and musculature to explore their potential impact on the performance of the arm-worn sensor. Individuals who were selected to participate in the protocol were asked to refrain from drinking alcohol and caffeine 24 h prior to data collection to prevent any external influence on hydration status. Following completion of the study, participants were provided electrolyte solution (Pedialyte) to replenish lost fluids and restore electrolyte balance. The diuretic-induced dehydration experimental protocol was approved by the Institutional Review Board at the University of Texas at Austin, with the ID STUDY00002585. Before participation, informed consent was obtained from all participants.

Data, Materials, and Software Availability. All study data are included in the article and/or *SI Appendix*.

ACKNOWLEDGMENTS. This research was supported by the US Office of Naval Research under Grant No. N00014-20-1-2112 and the NSF ASCENT Grant 2133106.

Author affiliations: [a]Chandra Family Department of Electrical and Computer Engineering, The University of Texas at Austin, Austin, TX 78712; [b]Department of Biomedical Engineering, The University of Texas at Austin, Austin, TX 78712; [c]Department of Kinesiology and Health Education, The University of Texas at Austin, Austin, TX 78712; [d]Department of Mechanical Engineering, The University of Texas at Austin, Austin, TX 78712; [e]Stretch Med Inc, Austin, TX 78750; [f]Department of Aerospace Engineering and Engineering Mechanics, The University of Texas at Austin, Austin, TX 78712; and [g]Texas Materials Institute, The University of Texas at Austin, Austin, TX 78712

Author contributions: M.J., S. Kang, S.B., J.K., J.W., K.D., T.H., S. Kim, E.C., and N.L. designed research; M.J., S. Kang, S.B., J.K., K.D., T.H., A.J., K.A., S. Kim, P.W., E.C., and N.L. performed research; M.J. contributed new analytic tools; M.J. analyzed data; N.L. PI; E.C., co-PI; and M.J., S. Kang, S.B., P.W., E.C., and N.L. wrote the paper.

1. R. A. Oppliger, C. Bartok, Hydration testing of athletes. *Sports Med.* **32**, 959–971 (2002).
2. D. C. Garrett *et al.*, Engineering approaches to assessing hydration status. *IEEE Rev. Biomed. Eng.* **11**, 233–248 (2017).
3. E. Jéquier, F. Constant, Water as an essential nutrient: The physiological basis of hydration. *Eur. J. Clin. Nutr.* **64**, 115–123 (2010).
4. S. M. Kleiner, Water: An essential but overlooked nutrient. *J. Am. Diet. Assoc.* **99**, 200–206 (1999).
5. P. Gopinathan, G. Pichan, V. Sharma, Role of dehydration in heat stress-induced variations in mental performance. *Arch. Environ. Health* **43**, 15–17 (1988).
6. N. A. Masento, M. Golightly, D. T. Field, L. T. Butler, C. M. van Reekum, Effects of hydration status on cognitive performance and mood. *Br. J. Nutr.* **111**, 1841–1852 (2014).
7. S. J. Montain, E. F. Coyle, Influence of graded dehydration on hyperthermia and cardiovascular drift during exercise. *J. Appl. Physiol.* **73**, 1340–1350 (1992).
8. T. Nishiyasu, X. Shi, G. W. Mack, E. R. Nadel, Effect of hypovolemia on forearm vascular resistance control during exercise in the heat. *J. Appl. Physiol.* **71**, 1382–1386 (1991).
9. L. E. Armstrong, Challenges of linking chronic dehydration and fluid consumption to health outcomes. *Nutr. Rev.* **70**, S121–S127 (2012).
10. A. M. El-Sharkawy, O. Sahota, D. N. Lobo, Acute and chronic effects of hydration status on health. *Nutr. Rev.* **73**, 97–109 (2015).
11. G. P. Bates, V. S. Miller, D. M. Joubert, Hydration status of expatriate manual workers during summer in the middle east. *Ann. Occup. Hyg.* **54**, 137–143 (2010).
12. R. P. Nuccio, K. A. Barnes, J. M. Carter, L. B. Baker, Fluid balance in team sport athletes and the effect of hypohydration on cognitive, technical, and physical performance. *Sports Med.* **47**, 1951–1982 (2017).
13. O. Najem, M. M. Shah, M. Zubair, O. De Jesus, *Serum Osmolality in StatPearls [Internet]* (StatPearls Publishing, 2024).
14. P. Wabel, P. Chamney, U. Moissl, T. Jirka, Importance of whole-body bioimpedance spectroscopy for the management of fluid balance. *Blood Purif.* **27**, 75–80 (2009).
15. O. R. Barley, D. W. Chapman, C. R. Abbiss, Reviewing the current methods of assessing hydration in athletes. *J. Int. Soc. Sports Nutr.* **17**, 1–13 (2020).
16. U. G. Kyle *et al.*, Bioelectrical impedance analysis–Part I: Review of principles and methods. *Clin. Nutr.* **23**, 1226–1243 (2004).
17. S. N. Cheuvront, R. W. Kenefick, Dehydration: Physiology, assessment, and performance effects. *Compr. Physiol.* **4**, 257–285 (2011).

18. S. F. Khalil, M. S. Mohktar, F. Ibrahim, The theory and fundamentals of bioimpedance analysis in clinical status monitoring and diagnosis of diseases. *Sensors* **14**, 10895–10928 (2014).
19. D. Kireev *et al*., Continuous cuffless monitoring of arterial blood pressure via graphene bioimpedance tattoos. *Nat. Nanotechnol.* **17**, 864–870 (2022).
20. H. Noddeland *et al*., A novel wearable bioimpedance sensor for continuous monitoring of fluid balance: A study on isotonic hypovolemia in healthy adults. *J. Clin. Monit. Comput.* **39**, 379–391 (2024).
21. G. Li, S. Wang, Y. Y. Duan, Towards conductive-gel-free electrodes: Understanding the wet electrode, semi-dry electrode and dry electrode-skin interface impedance using electrochemical impedance spectroscopy fitting. *Sens. Actuators B: Chem.* **277**, 250–260 (2018).
22. A. Piccoli *et al*., Discriminating between body fat and fluid changes in the obese adult using bioimpedance vector analysis. *Int. J. Obes.* **22**, 97–104 (1998).
23. S. Kumar, A. Dutt, S. Hemraj, S. Bhat, B. Manipadybhima, Phase angle measurement in healthy human subjects through bio-impedance analysis. *Iran. J. Basic Med. Sci.* **15**, 1180 (2012).
24. A. Piccoli, B. Rossi, L. Pillon, G. Bucciante, A new method for monitoring body fluid variation by bioimpedance analysis: The RXc graph. *Kidney Int.* **46**, 534–539 (1994).
25. US Department of Health Human Services *et al*., *NCHS Third National Health and Nutrition Examination Survey, 1988–1994* (Centers for Disease Control and Prevention, 1996).
26. K. R. Heavens, N. Charkoudian, C. O'Brien, R. W. Kenefick, S. N. Cheuvront, Noninvasive assessment of extracellular and intracellular dehydration in healthy humans using the resistance-reactance-score graph method. *Am. J. Clin. Nutr.* **103**, 724–729 (2016).
27. A. Moroni *et al*., Bioelectrical impedance vector analysis (BIVA) for the monitoring of body composition in pregnancy. *Eur. J. Clin. Nutr.* **76**, 604–609 (2022).
28. P. C. Martins, L. A. Gobbo, D. A. S. Silva, Bioelectrical impedance vector analysis (BIVA) in university athletes. *J. Int. Soc. Sports Nutr.* **18**, 1–8 (2021).
29. M. Carrasco-Marginet *et al*., Bioelectrical impedance vector analysis (BIVA) for measuring the hydration status in young elite synchronized swimmers. *PLoS ONE* **12**, e0178819 (2017).
30. T. Girma *et al*., Utility of bio-electrical impedance vector analysis for monitoring treatment of severe acute malnutrition in children. *Clin. Nutr.* **40**, 624–631 (2021).
31. D. H. Kim *et al*., Epidermal electronics. *Science* **333**, 838–843 (2011).
32. H. Li *et al*., E-tattoos: Toward functional but imperceptible interfacing with human skin. *Chem. Rev.* **124**, 3220–3283 (2024).
33. X. Huang, W. H. Yeo, Y. Liu, J. A. Rogers, Epidermal differential impedance sensor for conformal skin hydration monitoring. *Biointerphases* **7**, 52 (2012).
34. X. Huang *et al*., Epidermal impedance sensing sheets for precision hydration assessment and spatial mapping. *IEEE Trans. Biomed. Eng.* **60**, 2848–2857 (2013).
35. H. Cheng, Y. Zhang, X. Huang, J. A. Rogers, Y. Huang, Analysis of a concentric coplanar capacitor for epidermal hydration sensing. *Sens. Actuators A: Phys.* **203**, 149–153 (2013).
36. X. Huang *et al*., Biomedical sensors: Materials and designs for wireless epidermal sensors of hydration and strain. *Adv. Funct. Mater.* **24**, 3845 (2014).
37. S. Yang *et al*., Cut-and-paste manufacture of multiparametric epidermal sensor systems. *Adv. Mater* **27**, 6423–6430 (2015).
38. Y. Wang *et al*., Low cost, *mu*m-thick, tape-free electronic tattoo sensors with minimized motion and sweat artifacts. *npj Flexible Electron.* **2**, 6 (2018).
39. R. Matsukawa, A. Miyamoto, T. Yokota, T. Someya, Skin impedance measurements with nanomesh electrodes for monitoring skin hydration. *Adv. Healthcare Mater.* **9**, 2001322 (2020).
40. J. C. Spinelli *et al*., Wearable microfluidic biosensors with haptic feedback for continuous monitoring of hydration biomarkers in workers. *npj Digital Med.* **8**, 76 (2025).
41. S. Cho *et al*., A skin-interfaced microfluidic platform supports dynamic sweat biochemical analysis during human exercise. *Sci. Transl. Med.* **16**, eado5366 (2024).
42. K. Sel *et al*., Continuous cuffless blood pressure monitoring with a wearable ring bioimpedance device. *npj Digital Med.* **6**, 59 (2023).
43. S. Baidya, M. A. Ahad, Assessment of optimized electrode configuration for electrical impedance myography using genetic algorithm via finite element model. *J. Med. Eng.* **2016**, 9123464 (2016).
44. C. Gabriel, S. Gabriel, "Compilation of the dielectric properties of body tissues at RF and microwave frequencies" (Tech. Rep. ADA303903, Department of Physics, King's College London, London, UK, 1996).
45. Y. Asano, T. Tsuji, T. Okura, Segmental extracellular-to-intracellular water resistance ratio and physical function in older adults. *Exp. Gerontol.* **181**, 112278 (2023).
46. I. Lorenzo, M. Serra-Prat, J. C. Yébenes, The role of water homeostasis in muscle function and frailty: A review. *Nutrients* **11**, 1857 (2019).
47. S. Bhattacharya *et al*., A chest-conformable, wireless electro-mechanical e-tattoo for measuring multiple cardiac time intervals. *Adv. Electron. Mater.* **9**, 2201284 (2023).
48. International Electrotechnical Commission *et al*., Medical electrical equipment–Part 1: General requirements for basic safety and essential performance (2005), IEC 60601-1-2005.
49. J. R. Caton, P. A. Mole, W. C. Adams, D. S. Heustis, Body composition analysis by bioelectrical impedance: Effect of skin temperature. *Med. Sci. Sports Exerc.* **20**, 489–491 (1988).
50. M. J. Buono *et al*., The effect of ambient air temperature on whole-body bioelectrical impedance. *Physiol. Meas.* **25**, 119 (2004).
51. R. Hume, E. Weyers, Relationship between total body water and surface area in normal and obese subjects. *J. Clin. Pathol.* **24**, 234–238 (1971).
52. T. K. Mattoo, H. Lu, E. Ayers, R. Thomas, Total body water by BIA in children and young adults with normal and excessive weight. *PLoS ONE* **15**, e0239212 (2020).
53. A. Piccoli, Whole body-single frequency bioimpedance. *Cardiovasc. Disord. Hemodial.* **149**, 150–161 (2005).
54. H. C. Lukaski, C. B. Hall, W. A. Siders, Assessment of change in hydration in women during pregnancy and postpartum with bioelectrical impedance vectors. *Nutrition* **23**, 543–550 (2007).
55. L. E. Armstrong, Assessing hydration status: The elusive gold standard. *J. Am. Coll. Cardiol.* **26**, 575S–584S (2007).
56. B. Sun *et al*., Gas-permeable, multifunctional on-skin electronics based on laser-induced porous graphene and sugar-templated elastomer sponges. *Adv. Mater.* **30**, 180432 7 (2018).
57. B. Zhang *et al*., A three-dimensional liquid diode for soft, integrated permeable electronics. *Nature* **628**, 84–92 (2024).
58. L. B. Houtkooper, T. G. Lohman, S. B. Going, W. H. Howell, Why bioelectrical impedance analysis should be used for estimating adiposity. *Am. J. Clin. Nutr.* **64**, 436S–448S (1996).
59. A. C. Buchholz, C. Bartok, D. A. Schoeller, The validity of bioelectrical impedance models in clinical populations. *Nutr. Clin. Pract.* **19**, 433–446 (2004).
60. A. Piccoli, L. Pillon, F. Dumler, Impedance vector distribution by sex, race, body mass index, and age in the United States: Standard reference intervals as bivariate z scores. *Nutrition* **18**, 153–167 (2002).